Journal of Contaminant Hydrology 255 (2023) 104160

Contents lists available at ScienceDirect

Journal of Contaminant Hydrology

journal homepage: www.elsevier.com/locate/jconhyd

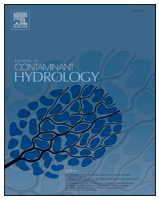

Transport-limited kinetics of phosphate retention on iron-coated sand and practical implications

Victoria Barcala [a,b,*], Alraune Zech [b], Leonard Osté [a], Thilo Behrends [b]

[a] Inland Water Systems, Deltares, 600 Daltonlaan, 3584 BK Utrecht, the Netherlands
[b] Department of Earth Sciences, Faculty of Geosciences, Utrecht University, 8 Princetonlaan, 3584 CB Utrecht, the Netherlands

ARTICLE INFO

Keywords:
Water treatment residuals
Phosphorous
Phosphorus sorbing materials
Reactive transport model
Mitigation measures
Recycled iron oxides

ABSTRACT

Iron-coated sand (ICS) is a by-product from drinking water treatment made of sand coated with ferric iron (hydr) oxides. It is considered a suitable material for large-scale measures for phosphate removal from natural and agricultural waters to prevent eutrophication. Previous studies demonstrated that the residence time of water must be very long to reach equilibrium partitioning between phosphate and ICS but specifics for application are missing. First, SEM-EDX images were used to support the conceptual assumption that P adsorption inside the coating is a transport-limited process. Second, a conceptual model of phosphate adsorption was proposed considering two types of sites: one type with fast adsorption kinetics and reaching equilibrium with the percolating solution, and another type for which adsorption is also reversible but described by pseudo-first-order kinetics. The latter is conceived to account for transport-limited adsorption in the interior of the coating while the former fraction of sites is assumed to be easily accessible and located close to the grain surface. Third, the kinetics of phosphate adsorption on ICS were quantitatively determined to describe and predict phosphate retention in filters under various flow conditions. The model was calibrated and validated with long-term column experiments, which lasted for 3500 h to approach equilibrium on the slowly reacting sites. The model reproduced the outflowing phosphate concentrations: the pronounced increase after a few pore volumes and the slow increase over the remaining part of the experiment. The parameterized model was also able to predict the time evolution of phosphate concentrations in the outflow of column experiments with different flow velocities, flow interruption, and in desorption experiments. The equilibrium partition coefficient for the experimental conditions was identified as 28.1 L/g-Fe at pH 6.8 and a phosphate concentration of 1.7 mg-P / L. The optimized first-order mass transfer coefficient for the slow adsorption process was 1.56 10^{-4} h^{-1}, implying that the slow adsorption process has a time scale of several months. However, based on the parameterized model, the slow adsorption process accounted for 95.5% of the equilibrium adsorption capacity, emphasizing the potential relevance of this process for practical applications. The implications for the design, operation, and lifespan of ICS filters are exemplarily illustrated for different scenarios.

1. Introduction

Particulate and dissolved phosphorus (P) losses from agriculture are a major threat to surface water quality (Bol et al., 2018; De Klein and Koelmans, 2011; Dupas et al., 2018; Kronvang et al., 2007; Schoumans et al., 2014; Withers et al., 2014). Because of the legacy P stored in the soil, reducing manure and fertilizer application is insufficient to reduce P loads reaching surface waters (Barcala et al., 2020; Bieroza et al., 2019; Gu et al., 2017; Sharpley et al., 2013). Phytoremediation, reducing the P in the soils by plant uptake, can reduce the legacy P but it will take decades before P losses to surface waters are reduced (Fiorellino et al., 2017; Koopmans et al., 2004; Lucas et al., 2021; Stoll et al., 2021). One option for short-term P load reduction is the implementation of permeable reactive barriers filled with iron (Fe)-containing materials. They can remove P from percolating water on its hydrological pathway from groundwater to surface waters (Das Gupta et al., 2012; Nur et al.,

Abbreviations: BET-SSA, Brunauer-Emmet-Teller specific surface area; DDL, diffuse double layer; Fe, iron; IC, ion chromatography; ICP-OES, inductively coupled plasma - optical emission spectrometry; ICS, iron coated sand; Mn, manganese; P, phosphorus; SEM-EDX, scanning electron microscope with energy dispersive x-ray spectroscopy.

* Corresponding author at: Inland Water Systems, Deltares, 600 Daltonlaan, 3584 BK Utrecht, the Netherlands.
E-mail address: victoria.barcalapaolillo@deltares.nl (V. Barcala).

https://doi.org/10.1016/j.jconhyd.2023.104160
Received 25 October 2022; Received in revised form 27 January 2023; Accepted 10 February 2023
Available online 13 February 2023

2014; Penn et al., 2011, 2017, 2020; Rittmann et al., 2011; Stoner et al., 2012). Particularly well-suited are byproducts from water treatment containing ferric iron (hydr)oxides given their easy availability and high binding affinity for P.

Iron-coated sand (ICS) and Fe sludge are residuals of deferrization of drinking water. A common procedure for deferrization is to oxidize dissolved Fe (II) and remove the produced Fe (hydr)oxides using sand filters. By this, an Fe coating develops around the sand grains resulting in ICS (Ippolito et al., 2011; Sharma et al., 2002; Van Beek et al., 2016, 2020). ICS and Fe sludge have been used to adsorb phosphate in soils, in filters around or at the end of tile drains, and in decentralized water treatment at farms (Boujelben et al., 2008; Chardon et al., 2021; Koopmans et al., 2020; Lambert et al., 2020; Moelants et al., 2011; Vandermoere et al., 2018; Zhang et al., 2022). The adsorption capacity of ICS is often underestimated as slow adsorption kinetics, controlled by intra-particle diffusion, are neglected (Ajmal et al., 2018; Koopmans et al., 2004; Willett et al., 1988). Iron (hydr)oxides in the coating of ICS are usually poorly crystalline or amorphous and exhibit a large specific surface area accounting for a high adsorption capacity (Chardon et al., 2012; Koopmans et al., 2020). However, the coating can be several hundreds of micrometers thick implying that the outer surface only represents a minor part of the total interfacial area. The outer surface of the ICS is in direct contact with the percolating water and the rates of adsorption are only controlled by the kinetics of the reaction. However, adsorption sites located in the interior of the coating can only be accessed via intra-particle diffusion.

The time scale of intra-particle diffusion is generally much longer than that of the surface reactions and, hence, the phosphate adsorption rates in the interior of the coating are transport limited. The long-term adsorption capacity of ICS can be underestimated when neglecting the slow transport-limited kinetics. The time scale of the slow adsorption exceeds the duration of typical batch adsorption experiments. Chardon et al. (2012) showed that the experimentally derived adsorption capacity of Fe sludge progressively increased in batch experiments over the duration of 21 days and in column experiments which lasted 238 days even further. The relevance of processes with different time scales was also reflected in the column experiments: P concentrations in the effluent quickly increased without reaching the inflow concentrations; instead, a quasi-steady state was reached at different P concentrations depending on the amount of Fe sludge in the column. This implies that the removal efficiency of Fe-containing filters depends on the contact time of the water in the filter being a function of pore volume and flow rates.

Lambert et al. (2020) and Zhang et al. (2022) investigated phosphate adsorption on ICS in batch and column experiments. Zhang et al. (2022) reported that the P outflow concentrations reached a quasi-steady state while the experimental data in Lambert et al. (2020) only represent fast P adsorption as experiments were stopped before the quasi-steady state was reached. In both studies, the Bohart-Adams model was applied to describe the breakthrough curves of phosphate. The Bohart-Adams model only accounts for the kinetics of one irreversible adsorption reaction and, consequently, its performance is limited when dealing with processes proceeding with different paces. Lambert et al. (2020) parameterized the model for the pronounced increase in dissolved P concentrations until adsorption equilibrium is reached for the fast-reacting sites. However, when changing flow velocities, the contribution of the slow adsorption processes to P retention varied and, consequently, column experiments with different flow velocities required individual optimization of model parameters. In particular, the obtained P adsorption capacity was larger for the column operated at slow flow than that at fast flow, and both were significantly larger than the capacity obtained in a 1-day batch experiment. Furthermore, Lambert et al. (2020) reported that a pilot filter operated with intermittent resting periods performed better than when operated with continuous flow for the same treated volumes. These results demonstrate that slow adsorption kinetics need to be considered for optimizing the operation of ICS filters and the need for a reactive transport model, which accounts for the kinetics of both, fast and slow, adsorption processes. Here and in the following, the term 'kinetics' is used in the broadest sense, encompassing rates and mechanisms of chemical reactions as well as transport processes such as diffusion (Zhang, 2008).

The objective of this study was to develop a quantitative model for phosphate adsorption on ICS that can adequately account for slowly proceeding phosphate adsorption, which can be easily implemented and applied to optimize the operation of ICS containing filters. Electron microscopy in combination with energy-dispersive X-ray spectroscopy was used to illustrate the model consideration that phosphate retention in the interior of the iron coating is transport limited. A process-based physical model, including kinetic adsorption of phosphate on ICS, was parameterized using long-term column measurements. The model represents the slow kinetics dominated by the diffusion of phosphate inside the ICS coating and the fast adsorption on the outer surface of the ICS. It is shown that the model can be a valuable tool to optimize the design and operation of ICS filters over their whole lifespan with different flow velocities and intermittent flow regimes.

2. Materials and methods

2.1. Iron coated sand

The ICS used in this study was provided by AquaMinerals BV (https://aquaminerals.com/en/). The material was obtained from one mixed batch originating from different drinking water production sites. The ICS received no pre-treatment, was obtained air-dried, and stored in the dark at room temperature. The ICS contained on average 127.2 mg/g Fe, 9.4 mg/g Mn, 0.5 mg/g S, 9.6 mg/g Ca, and 0.9 mg/g P ($\pm$ 0.1 mg/g standard deviation) determined by total destruction. The Brunauer-Emmet-Teller specific surface area (BET-SSA) was 71.2 m^2/g and was determined using argon gas with an ASiQwin instrument (Quantachrome Instruments). In addition, the pore size distribution in the ICS was determined with the BET-SSA analysis, nano-pores with a diameter between 0.42 and 2.00 nm were related to 54% of the specific surface and mesopores between 2.00 and 50.0 nm to 46%. Details of the measurement are specified in the *Supplement Material.*

2.2. Column experiments

We performed flow experiments in 3 columns, named I, II, and III. The three columns were made from transparent polyethylene tubes of 30.8 cm height and 4.3 cm internal diameter. The column dimensions were selected accounting for dispersivity and reducing boundary flow effects along the tube walls (Bromly et al., 2007; Lewis and Sjöstrom, 2010). The reactive core of the columns contained 30 g of ICS and 300 g of quartz sand, both with grain diameters between 1.18 mm and 2.00 mm. The ICS was mixed with quartz sand to reduce the breakthrough times by maintaining column dimensions according to recommendations based on previous column experiments (Bromly et al., 2007; Lewis and Sjöstrom, 2010). Quartz sand is commonly used as an inert filling material in column experiments (Chardon et al., 2012; Jerez and Flury, 2006; Mystrioti et al., 2015; Pérez-López et al., 2007) and it is assumed that it does not contribute to phosphate retention in the columns. This implies that equilibrium constants or partition coefficients *Kp* [*L/g*] determined for the whole stationary phase can be normalized to the content of ICS. Two layers of 180 g quartz gravel ($>$ 2 mm) were added at the top and bottom of the columns to improve the flow distribution. The columns were fed from the bottom via tubes of 0.8 mm internal diameter, which were also used for the outflow. The total volume of the tubing was 14.5 cm^3 and taken into consideration in the parametrization of the models. The inflow solution was stored in 10 L glass bottles protected from the light with black plastic bags. The bottles' cups were modified to work as Mariotte bottles (Maroto et al., 2002) to maintain a constant head pressure of approximately 2 cm above the columns

assuring full saturation. A peristaltic pump (Masterflex L/S) with the corresponding tubing (13 L/S, Masterflex) was used for each column to maintain a constant flow. The flow rate at the given pump speed was checked prior to the experiments. Different flow regimes were used in the three different columns, including constant flow at various velocities, but also variable flow patterns. Furthermore, one column was used for a desorption experiment. The chosen flow rates correspond to the range of flow velocities measured in field applications of ICS for retaining phosphate in drainage systems (Barcala et al., 2022; Groenenberg et al., 2013). The flow rate in column I was 0.65 mL/min for 3500 h (over 560 pore volumes). For the first 1440 h, column II was running in parallel to column I with a flow rate of 0.65 mL/min. Afterward, the flow rate was reduced to 0.39 mL/min for600 hours. We also aimed to maintain the flow rate in column III at 0.65 mL/min during the first 1440 h of the experiment but clogging occurred The cause of the clogging was the obstruction of the outflow tube by particles. The issue was solved by flushing the tube with water. The tube was cleaned six times during this period. Although unintended, clogging provided the opportunity to study the effect of interrupted flow and the data were included in this study. After the problematic tube had been replaced for a new one, column III was used without interruptions during 720 h in a desorption experiment at 0.65 mL/min. In addition, a second adsorption experiment with a flow rate of 0.39 mL/min was performed in column III for the last 600 h. Adsorption experiments were performed with a solution prepared from demineralized water containing 1.70 ± 0.05 mg /L P in the form of monobasic sodium phosphate solution. In order to maintain the ionic strength constant 0.10 M NaCl was also added. The desorption experiment was performed with 0.10 M NaCl without P. The pH was adjusted with NaOH to 6.80 ± 0.05 and controlled weekly in the inflow and outflow. The retention times at 0.65 mL/min where 375 min in column I, 329 min in column II, and 301 min in column III.

Samples were collected every 8 h with an autosampler (SC-4DXS, Elemental Scientific) in 50 mL PE centrifuge tubes pre-acidified with 1 mL 6 M HCl. The volume collected by the autosampler during a sampling interval served as a periodic control of the flow rate. P concentrations [mg/L] (equivalent to mg-P/L) in samples were measured photometrically (DR3900, Hach), as samples form a blue complex that follows Beer's law when reacting with an acidified ammonium heptamolybdate solution and freshly added ascorbic acid (Murphy and Riley, 1962). For the first 40 days, one sample per day was analyzed with ICP-OES (Avio 500, Perkin-Elmer) as an independent measurement. Because Stanmod (Simunek et al., 1999; Van Genuchten et al., 2012) can only deal with constant flow velocities, the data series from columns I and II were quality checked and a few points that were affected by flow rate reductions were removed. Preliminary tracer experiments were performed in all columns to determine pore volumes and porosities. For this 0.10 M NaCl solution was used containing additionally 0.10 M NaBr. The flow was 0.65 mL/min. Samples were taken manually every 12 min for 9 h. Electric conductivity (EC) was measured and bromine (Br) concentrations were determined by ion chromatography (ICS6000, Thermo Scientific) to determine the breakthrough of the non-reactive tracer.

2.3. ICS imaging techniques

SEM-EDX analyses were performed to investigate the structure of the ICS coating and to examine the P distribution. This was done to illustrate the conceptual idea of transport-limited uptake of P inside the coating. SEM micrographs and elemental maps were made for fresh ICS and for ICS after adsorption from column III. The grains were embedded in resin and polished to investigate cross-sections. Secondary electron and backscattered electron images were acquired on a SEM (EVO 15, Zeiss), using the SmartSEM user interface (v 6.06). (Semi-) qualitative chemical compositions were obtained using EDX (Esprit v. 2.1, Bruker XFlash).

2.4. Reactive transport model

The conceptual model was parametrized into a reactive transport model using the advection-dispersion equation, and including two reactive adsorption terms. In order to account for different adsorption rates, two types of adsorption sites were included: fast-reacting sites for which the reaction progresses in time scales shorter than the hydraulic residence and conceived to reach equilibrium with the P concentrations in the mobile phase, and sites for which the adsorption is kinetically controlled. Adsorption of P to ICS is conceived as a reversible process. The fast adsorption process was characterized by linear adsorption using an equilibrium partition coefficient (*Kp*). The assumption of linearity is warranted at relatively low P concentrations as the relative occupation of adsorption sites remains low in equilibrium and the concentrations of occupied sites can be neglected in the mass balance for the reactive sites. When the content of vacant sites can be assumed to be constant, the kinetics of P adsorption to ICS simplify to pseudo-first-order rate laws for P adsorption and desorption solely depending on the P concentration in the mobile phase and P adsorbed to slowly reacting sites, respectively. The derivation of the equations is available in the *Supplementary Material.*

Based on this conceptual model, the corresponding mass balance equations for P in the mobile and stationary phase in one-dimension read:

$$\left(1+\frac{\rho f K_p}{\theta}\right)\frac{\partial c}{\partial t} = D\frac{\partial^2 c}{\partial x^2} - \frac{v\partial c}{\partial x} - \frac{\rho\alpha}{\theta}\left(s_{eq} - s\right) \tag{1}$$

$$\frac{\partial s}{\partial t} = \alpha\left(s_{eq} - s\right) \tag{2}$$

Where c is the P concentration [mg/L] in the mobile phase, x is the longitudinal coordinate [cm], t is time [h], ρ is the bulk ICS density [g/L], f is the fraction of fast reacting sites, θ is the porosity, Kp is the equilibrium constant or partition coefficient [L/g], D is the dispersion coefficient [cm^2/h], v is the pore-water velocity equal to the darcian flow velocity divided by porosity [cm/h], α can be attributed to the rate constant for P desorption but also conceived as the exchange coefficient between the stagnant and mobile phase [1/h] (see *Supplementary Material* for details), and s is the P concentration in the solid phase for which adsorption is kinetically controlled [mg/g]. s_{eq} is not an extra variable but the equilibrium concentration in the solid phase of the slow sites equal to $K_p(1-f)c$. The concentration of P bound to the fast-reacting sites, being in equilibrium with the percolating solution, is not a state variable in the model but is calculated based on the product of f, c, and Kp.

2.5. Model solution and parameter estimation

At constant flow and constant P concentrations in the inflow, the equation system has an analytical solution that has been implemented in the code Stanmod (Simunek et al., 1999; Van Genuchten et al., 2012). We used the module CXTFIT (Toride et al., 1995) for parameter estimation that minimizes the root mean squared error (RMSE) between the experimental and calculated concentrations.

The hydraulic properties, pore-water velocity v, and the porosity θ, of each column, were determined separately from the tracer experiments. We identified adsorption parameters f, α, and Kp by calibrating the P concentrations in the effluent of column I over the first 690 h of the experiment. During the first 690 h, ICP-OES was used to measure P concentrations. Afterward, the photometric method was used, having a higher analytical uncertainty and some irregularities occurred in the flow such as short periods of flow decrease. These points were still included in the data series as the long-term P retention could still be observed. The model was validated by calculating RMSE and the coefficient of determination (R^2) for the effluent concentrations in column I over the whole experiment duration of 3500 h, the concentrations in

column II during the first1440 hours, and the P concentration of the last 600 h of column III. In the latter case, the experiment was conceived as an independent P-removal experiment and any possibly remaining P in the column after the preceding adsorption and desorption experiments was neglected.

For variable flow rates, eqs. 1 and 2 do not have an analytical solution. Therefore, we implemented a numerical solution using the R-packages ReacTran and deSolve (Soetaert and Herman, 2009; Soetaert and Meysman, 2012; Soetaert and Petzoldt, 2010). The model in R was fed with the calibrated parameters obtained from column I. The dynamic model allows to validate the experiment with intermittent flow velocities (flow interruptions). We calculated the RMSE and R^2 between the parametrized model's results and the effluent of column III during the flow interruptions and for the desorption experiments. The model is available at https://github.com/victoriabarcala/ICS_adsorptionmodel.

The optimized value for *Kp* is conditional and accounts for the affinity of sorption sites for P at the given conditions plus the total concentration of sites. For example, phosphate adsorption to ferric iron (hydr)oxides depends, among other factors, on pH and ionic strength (Morel and Hering, 1993). To assess the possibility to extrapolate the

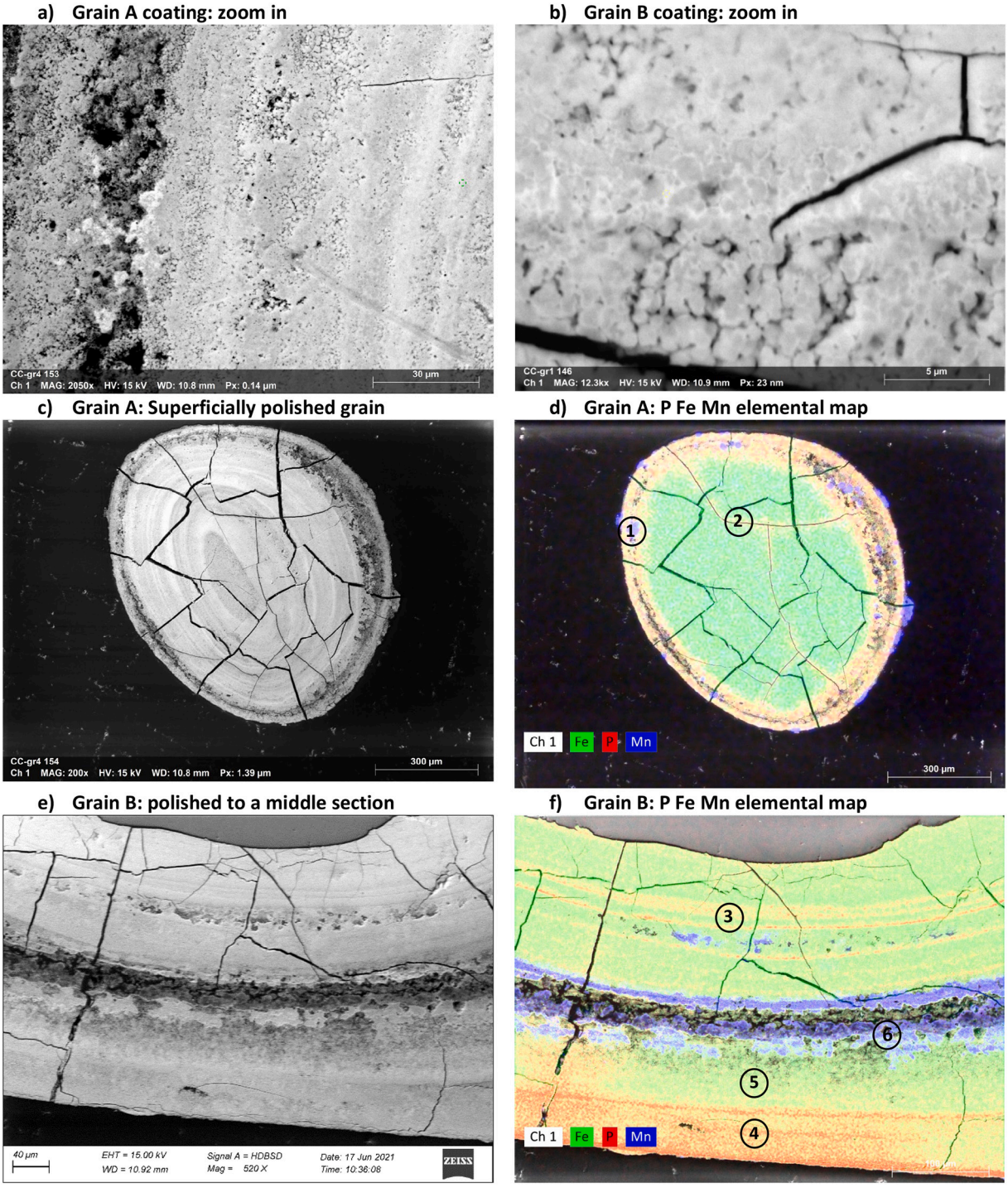

Fig. 1. SEM-EDX images of ICS grains from column III after adsorption experiments. While grain A (c&e) is superficially polished, grain B (d&f) shows a cross-section. Electric high tension (EHT), scales and working distances are indicated on each image.

model to other conditions, we compared the obtained value of *Kp* with calculated values based on surface complexation models. For this, the generic diffuse double layer (DDL) model parameterized by Dzombak and Morel (1991) for hydrous ferric oxide and implemented in MINEQL (version 5.0) was used to calculate the P partition for the given experimental conditions and calculate the corresponding *Kp*.

2.6. Practical example

We used the numerical R-model to set up a practical example illustrating the implications of considering the kinetics of P adsorption in the application of ICS. The example considers the use of ICS to remove dissolved P from water at the effluent of tile drains installed in an agricultural area. Thus, the chosen setting parameters are close to reality. The average P concentration in the incoming water is assumed to be 1.0 mg/L and the target P concentration should be below 0.15 mg/L after passing the filter. This concentration was chosen as the Dutch implementation of the water framework directive establishes a 0.15 mg/L limit in total phosphorus for open regional waters such as ditches (Fraters et al., 2021). The filter has a porosity of 0.50, 1770 g/L bulk density with a Fe concentration of 0.13 mg-Fe/g-ICS, and the filter dimensions are 40x40x40 cm. The flow rate during operation is 4 L/h. We compare the efficiency of four different filter operations: (i) continuous flow, (ii) resting 3 months a year (during summertime), (iii) resting 1 week, and (iv) 2 weeks per month.

3. Results

3.1. Microscopy and ICS analysis

The coatings around ICS grains have a thickness between 100 μm and 300 μm and often exhibited an anisotropic structure (Fig. 1). The Fe-rich coating is traversed by Mn-rich layers typically exhibiting a higher porosity (Fig. 1-a and 1-b). In the investigated coatings, EDX analyses show a distinct P enrichment in their outer part (Fig. 1-d, highlight point 1 and 1-f, point 4, EDX spectra are available in the supplementary material). In the outer parts (Fig. 1-f point 4), comprising about 20% of the coating, P/Fe ratios were around 0.040 and about 10 times larger than in the P-poor areas (Fig. 1-f, point 5) with ratios about 0.004. Additionally, several thin layers with elevated P/Fe ratios were identified close to the core (Fig. 1-f point 3). No P was detected in the Mn-rich areas (Fig. 1-f point 6). The coatings were disrupted by several cracks. Some of the cracks exhibited P enrichments at the margins (Fig. 1-d, point 2). However, most cracks seen on Figs. 1-c and 1-d do not show this feature and were possibly created when vacuuming the sample before SEM analysis.

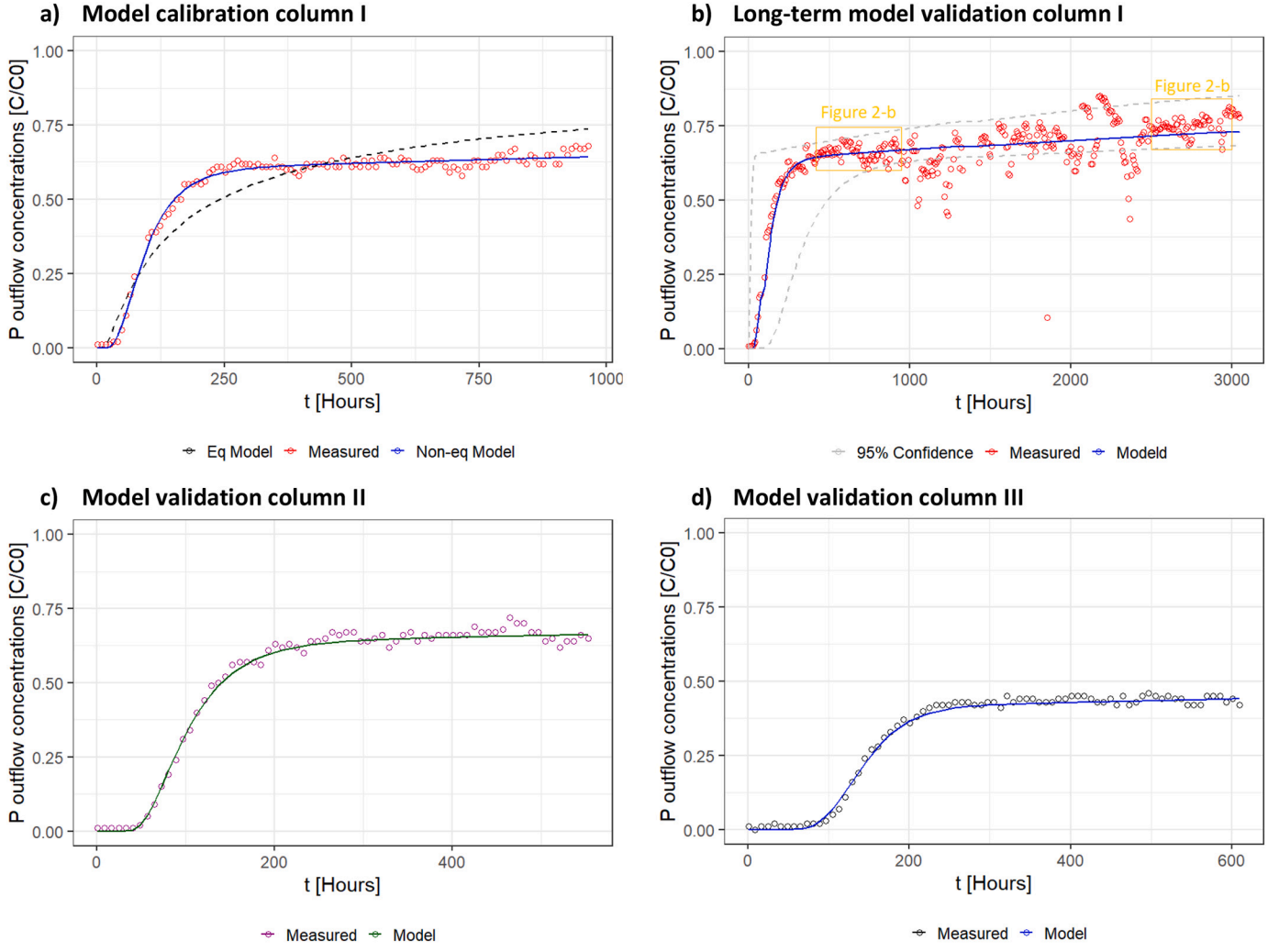

Fig. 2. Results from continuous flow adsorption experiments and reactive transport model implemented in Stanmod with different pore-water velocities, a) model calibration column I at v = 4.92 cm/h the black dashed line in a shows the best fit using a one-site equilibrium adsorption model, b) long-term validation in column I at v = 4.92 cm/h, c) validation in column II at v = 5.55 cm/h, and d) validation in column III at v = 3.66 cm/h. The black dashed line in a shows the best fit using a one-site equilibrium adsorption model. The inflow concentration C0 is 1.70 mg/L.

3.2. Adsorption experiments

The general features of the time evolution of P concentrations in the effluent of column I were representative of the adsorption experiments with all columns. After an initial increase in outflow concentrations, a quasi-steady-state was reached at concentrations lower than in the inflow solution (Fig. 2-a). Between hours 240 and 960, the outflow concentrations were about 1.05 mg/L for column I representing 62% of the inflow concentration. The pronounced increase in P concentrations occurred significantly later than the hydraulic retention time, reflecting the retention of P via adsorption also at the beginning of the experiment. A one-site model assuming equilibrium partitioning of P cannot trace the measured effluent P concentrations (Fig. 2-a). In particular, the model cannot produce a prolonged period of virtually constant concentrations below inflow concentration. In contrast, the two-site model based on eqs. 1 & 2 was able to reproduce the features of the concentration curve including the pronounced increase after the first days of operation and the plateau concentration reached after about 240 h (Fig. 2). The equilibrium constant for the fast sites *Kp* was identified with 0.155 L/g for the ICS-sand mix and 3.57 L/g for pure ICS with 95% confidence intervals [1.15, 5.98] L/g (Table 1). The small value for the fraction of fast adsorption sites *f*, 0.045, indicates that most adsorption sites were located within the Fe coating. The small value for the mass transfer coefficient α, 1.56 10^{-4} h^{-1} reflects the slow transfer process.

Hydraulic parameters have been identified separately through tracer tests, which showed recovery rates of 97%. The dispersion coefficient D was fitted to 30 cm^2/h, and the Peclet number to 5.05. The tracer test curves and sensitivity analysis of the parameters in Stanmod are available in the *Supplementary Material*.

Table 1
Summary of tracer experiment results, as well as results of model calibration and validation for column experiments.

Tracer experiment			
	column I	**column II**	**column III**
Hydraulic retention time (min) (at 0.65 mL/min)	375	329	301
Porosity Θ	0.55	0.49	0.44
Pore volume (mL)	243	241	196
Flow velocity v (cm/h) at 0.65 mL/min	4.92	5.55	6.09
Flow velocity **v** (cm/h) at 0.39 mL/min	–	3.33	3.66

Calibration, Fig. 2-a			
	***Kp* [L/g] ***	**α [1/h]**	***f***
Column I, adsorption, 4.92 cm/h, 960 h	0.155	1.56e-4	0.045
Lower 95% confidence interval	0.05	1.47e-4	0.012
Upper 95% confidence interval	0.259	1.65e-4	0.076
R^2	0.988		
RMSE (mg/L)	0.03		

Validation		
	r	**RMSE (mg/L)**
Column I, adsorption, 5.55 cm/h, Fig. 2-b, 3024 h	0.88	0.138
Column II, adsorption, 5.55 cm/h, Fig. 2-c	0.99	0.058
Column III, adsorption, 3.66 cm/h, Fig. 2-d	0.98	0.059
Column III, stop-flow, 6.09 cm/h, Fig. 4-a	0.91	0.182
Column III, desorption, 6.09 cm/h, Fig. 4-b	0.96	0.074

* *Kp* is of the ICS-sand mix. The *Kp* of the ICS is 3.57 L/g, 95% confidence intervals [1.15, 5.98] L/g. For the equilibrium model, parameter fitting yielded unrealistic values in order to approach the quasi steady state concentrations after the initial rise in P concentrations: K_p was2.2 × 10^{34} L/g with 95% CI [−5.6 × 10^{35}, 6.1 × 10^{36}] L/g, D was 0.169 × 10^{38} cm with 95% CI [−0.434 x10^{39}cm, 0.468 x10^{39}cm], and R^2 was 0.82.

The model was first validated for column I by modeling the whole duration of the experiment (3500 h) beyond the first 960 h for which parameters were determined. The larger deviation between observed and calculated data is associated with an increase in analytical uncertainty due to the switch in the analytical method. Notably, the model accounted for the slow increase in P concentration as the system was approaching equilibrium (Fig. 2-b and 3-b). The change in outflow concentration due to the slow adsorption process is emphasized when comparing concentrations at an early and a late stage of the experiment in Fig. 3-b.

By the end of the experiment the effluent concentration in column I reached around 1.35 mg/L, corresponding to a P content in the solid phase of around 2.16 mg/g-ICS or 17.0 mg/g-Fe (0.03 P/Fe molar ratio). At this moment, the effluent concentrations were still below the inflow concentration implying that equilibrium was not reached. With the model we extended the running-time to two years, the projected outflow P concentration was 1.60 mg/L (94% of the inflow concentration) and the concentration in the solid phase was 6.00 mg/g-ICS or 47.02 mg/g-Fe. This value is close to the expected P loading in equilibrium ($s_{eq_{tot}} = c \bullet K$) of 6.07 mg/g-ICS or 47.57 mg/g-Fe (0.09 P/Fe molar ratio). We thus conclude that when the experiment ended, about 36% of the equilibrium concentration in the solid was reached.

We obtained more validation results by running the transport model for the other columns with the parameters *f*, α, and *Kp* identified for column I and the specific hydraulic parameters for each column. The model reproduced very well the effluent concentrations from column II (Fig. 2-c, Table 1) and column III (Fig. 2-d, Table 1) at different flow velocities. When column III reached quasi-steady-state the effluent concentrations were around 0.75 mg/L and significantly lower than the values reached in columns I and II with higher flow velocities. The flow rate in column II was decreased to 0.39 mL/min to investigate the effect of changing the flow rate on the P concentrations at quasi-steady-state. As expected, P concentrations decreased and stabilized at a new quasi-steady-state about 0.2 mg/L lower than effluent concentrations of column I (Fig. 3-a) illustrating the increasing effect of the slow adsorption process at increasing contact time.

Stop-flow situations were studied with the early column III data where unintended flow interruptions due to obstructions in the outflow tube. Our conceptual model predicts the transfer of P from fast to slow sites due to diffusion during stopped flow accompanied by decreasing concentrations of dissolved P in the column. Consequently, we expect lower P concentrations in the effluent after resuming the flow, similar to the initial phase of the column experiments. Indeed, at most flow interruptions, the P concentrations in the effluent followed the expected pattern and the previous concentrations were approached with some retardation (Fig. 4-a).

The numerical model was able to reproduce the stop flow regime in column III (R^2 0.91, Table 1). Figs. 4-c and 4-d show the calculated time evolution of the concentrations in the mobile and stationary phases inside column III. The flow interruptions were reflected in a pronounced decrease in dissolved P concentrations, in particular at the lower part of the column where the solution was entering. The continuation of P adsorption during stopped flow resulted in increasing contents of adsorbed P (Fig. 4-d). After 1481 h but only 693 h with flow, 1.39 mg/g-ICS of P were adsorbed, being 22% of the equilibrium concentration. Later, 0.57 mg/g (about 40% of the previously adsorbed mass) was recovered in the desorption experiment, in 720 h. The transfer of phosphate from fast to slowly reacting sites becomes less efficient when the slow sites approach equilibrium as the distance from equilibrium ($s_{eq} - s$), which drives the transfer, becomes smaller. During the desorption experiment in column III, the effluent concentrations decreased and reached a quasi-state concentration of about 0.4 mg/L (Fig. 4-b). This can be attributed to the release of P from the slow-reacting sites. The quasi-steady-state behavior was well reproduced by the model while the agreement between the model's results and observation is lower in the transition period as concentrations drop faster than

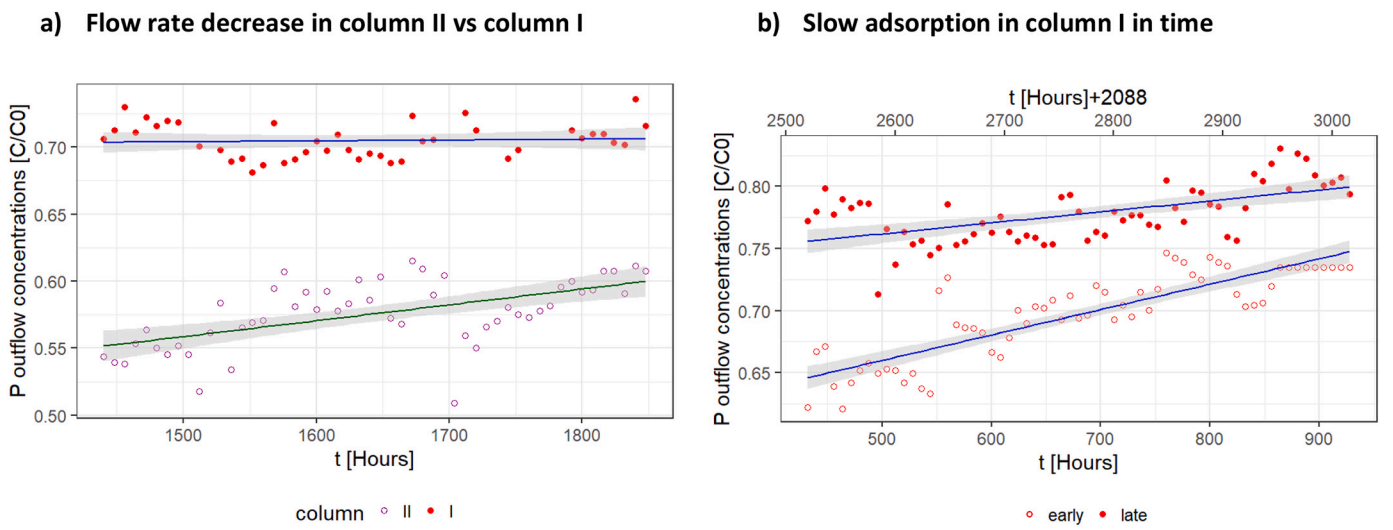

Fig. 3. Measured concentrations during slow adsorption. a) Effect of flow rate decrease: column II with v = 3.33 cm/h and column I with v = 4.92 cm/h at a late stage of the experiment. b) Differences in the slow adsorption in column I with time: steeper increase at early times (hour 460 to 930) compared to late time (hours 2520 to 3020). Shaded areas indicate 95% confidence interval of the trend lines. The inflow concentration C0 is 1.70 mg/L.

predicted. The desorption process was modeled with the same mass transport rate (α), implying that transport limitations also retard desorption. Consequently, techniques only relying on P desorption may not be efficient for phosphate recovery due to the long time scale of desorption.

4. Discussion

4.1. Expediency of the two-side model

Considering transport-limited kinetics for the adsorption process in a two-site model was crucial to reproduce P outflow concentrations of long-term column experiments. The two-site adsorption model proved suitable to describe and predict P retention for different operational scenarios, including the variations in constant flow velocities, interrupted flow, and desorption. Although parameterized for one column experiment for a limited duration, it was able to reproduce the features of the observed effluent P concentrations in all other experimental settings.

In particular, quasi-steady-state concentrations, being key in determining the P removal throughout the experiments, were well reproduced at all flow conditions. Only during transient flow periods, when resuming the flow or after abrupt changes in inflow concentrations, the predictive capability of the model was lower. The apparent delay in the predicted P concentrations in the outflow after flow interruptions or in the desorption experiment can be partially attributed to the remaining solution in the inert gravel layer at the top of the column. This layer is not included in the dynamic model and dissolved P concentrations do not change during no-flow concentrations due to the absence of ICS.

The reactive model does not include an explicit description of the intra-coating diffusion process. Instead, the transport limitation is accounted for in the parameter α, which can be interpreted as an exchange coefficient between the stagnant phase (intra-coating porosity) and a mobile phase (see Supplementary Material for details). An equivalent approach was used before to describe phosphate desorption from soil particles (Koopmans et al., 2004). Adsorption was considered to be reversible and to follow a linear isotherm. The desorption experiment demonstrates that adsorption of P to ICS is reversible. Studying P adsorption onto ICS, Lambert et al. (2020) employed Langmuir and Freundlich isotherms for dissolved P concentrations in the range of 0–1200 mg/L. Both isotherms may be approximated by a linear relationship at concentrations lower than 20 mg/L. In our study, dissolved P concentrations remain below levels at which deviation from linearity is typically reported for P adsorption isotherms and solid phase contents remain below the saturation capacity, for example, reported for ferrihydrites (Wang et al., 2013). The linear approximation is justified in the context of applying ICS for P removal in drainage water in the Netherlands which typically have soluble reactive phosphate concentrations below 2 mg/L P (Rozemeijer et al., 2014).

4.2. Model parameters

Despite the dilution of ICS with non-reactive sand and the long duration of the experiment, equilibrium between dissolved and adsorbed P was not achieved. The correlation of parameters *f, Kp* and *α* complicate the unequivocal determination of each parameter. Particularly, the pronounced, initial increase in P concentrations can be reproduced with infinite combinations of *f* and *Kp*. Similarly, quasi-steady-state concentrations are controlled by a combination of *Kp* and *α*. However, the very slow increase in dissolved P concentrations after the initial increase constraints *α*, and allows a robust estimation of the partition coefficient *Kp* and consequently *f*.

The major part of the adsorption capacity lays inside the coating. The fraction of fast adsorption sites *f* was only 4.5% reflecting the small number of sites at the outermost layer of the coating, which is in direct contact with the porewater. SEM-EDX analyses support the conceptual assumption that P adsorption inside the coating is a transport-limited process: P is not homogeneously distributed but enriched in the outer part of the coating and in some narrow layers inside the coating. Although SEM-EDX micrographs indicate the possibility of P transport through macro pores in the coating, transport into the bulk of the coating is likely controlled by diffusion through the intra-porosity of the Fe precipitates, which is supposed to be faster than solid diffusion (Willett et al., 1988). The Fe-(hydr)oxides in the coating are expected to be of low crystallinity comparable to the structure of ferrihydrite. A pore width between 0.42 and 50 nm was obtained from BET analyses being about half of them mesopores (2–50 nm). The range of pore widths indicates that the majority of pores are sufficiently large to allow for diffusion of hydrogen- and dihydrogen phosphate with Stoke's radii of 0.35 and 0.26 nm, respectively(Hong et al., 2009). The relevance of mesopores for P adsorption was demonstrated by Suresh Kumar et al. (2017) who found, at low P concentrations, a linear relationship between the mesopore BET specific surface area and P adsorption in granulated activated carbon coated with Fe oxides. The pore size values

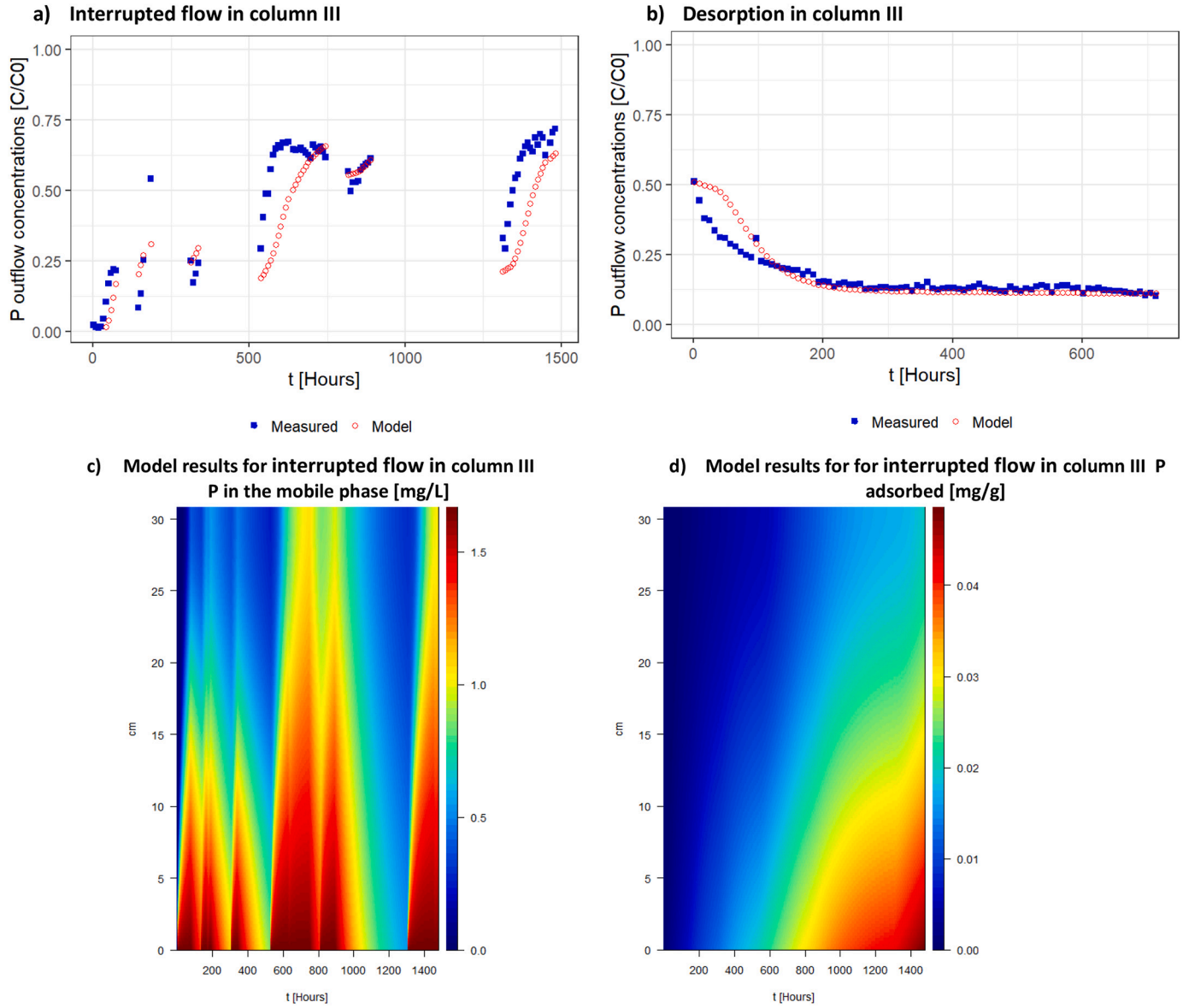

Fig. 4. Column III results of P concentrations. The inflow concentration C0 is 1.70 mg/L. a) Measured and numerically modeled P in the outflow during interrupted flow, b) measured and modeled outflow P during desorption, c) P in the mobile phase along the column during the experiment with flow interruptions, d) adsorbed P content along the column during the experiment with flow interruptions.

for 2-L and 6-L ferrihydrite obtained by Wang et al. (2013) range from 1.6 to 4.4 nm. The relatively large variability of pore sizes measured for ICS can be explained by changing conditions in the surrounding water during the growth of the coating. The composition of the inflow water in the sand filter can be variable as well as the position of the grains in the filter caused by backflushing. Both types of events might affect the structure of Fe precipitates in the sand filters (Jentzsch and Penn, 2006; Van Beek et al., 2020) and hence pore size distribution.

Based on the optimized mass transfer coefficient α of 1.56 10^{-4} h^{-1} the time scale of the slow adsorption process is about 6400 h. Consequently, the required equilibration times for determining *Kp* in batch experiments using ICS grains would be much longer than the duration of the column experiments. This implies that column experiments in combination with reactive transport modeling appear to be more efficient for estimating the equilibrium partition coefficient of P for ICS. Furthermore, there are practical limitations for the use of batch experiments to constrain *Kp* for ICS as the coating can be lost during shaking and reduced to small pieces (Chardon et al., 2012).

The obtained value of *Kp* compares well to those reported in other studies. We found $Kp = 3.56$ L/g for pure ICS or 28.1 L/g-Fe (deduced from the estimated *Kp* for the ICS-sand mixture, see Table 1) at an equilibrium P concentration of 1.70 mg/L, corresponding to P contents of 6.06 mg/g-ICS or 47.7 mg-P/g-Fe (0.09 P:Fe molar ratio) in the solid phase. Wang et al. (2013) report a value of 52.3 mg/g-Fe for 2-L ferrihydrite powder in equilibrium with 1.0 mg/L dissolved P, while Chardon et al. (2012) obtained 56.83 mg/g-Fe for iron sludge from drinking water treatment in column experiments at 3.95 mg/L after 283 days (6792 h). Lambert et al. (2020) report a maximum adsorption of 16.3 mg/g-Fe for ICS in a column experiment after 280 days (6720 h) and a 20 mg/L inflow concentration. Surprisingly, the value is lower than ours, as the inflow concentrations in Lambert et al. (2020) experiment were considerably higher, and the duration of their experiment was longer compared to our experiments. However, the amount of ICS in the column used by Lambert et al. (2020) was 195 g, about seven times larger than in this study at a comparable flow rate of 2.53 cm/h. The experiment only captured the pronounced, initial increase in effluent concentrations and not the prolonged slow increase afterward. In this stage of the experiment, adsorption at the slow sites is of lower relevance

leading to lower values when calculating an apparent partition coefficient. According to our results, the equilibrium solid concentration at a dissolved P concentration of 20 mg/L is 120.7 mg/g-Fe. When only considering the fraction with fast rates (4.5% of total adsorbed), 5.5 mg/g-Fe are reached, which is close to the value obtained by Lambert et al. (2020) in their batch experiments with 24 h equilibration time (5.93 mg/g-Fe). Per surface area, the maximum P adsorption we obtained was 0.084 mg/m^2 which is very similar to the value of 0.081 mg/m^2 obtained by Koopmans et al. (2020) for Fe-containing precipitates from drinking water treatment, which was used 14 months for soil amendment.

The optimized partition coefficient *Kp* is conditional and expected to depend on pH, ionic strength, and the presence of other ions adsorbing to ICS. The model was calibrated and validated for pH 6.80 ± 0.05, 0.10 M ionic strength, 1.70 ± 0.05 mg/L inflow concentration, and no competing ions. Higher pH reduces P adsorption (R. Zhang et al., 2022) due to competing OH^- ions and a decreasing surface charge at higher pH. Differences in ionic strengths can alter P adsorption by mitigating electrostatic effects. The effect of pH and ionic strength could be accounted for when applying surface complexation models including the acid-base chemistry of surface sites and electrostatic corrections such as the generic DDL model parameterized by Dzombak and Morel (1991) for hydrous ferric oxides (HFO). The generic DDL provides a *Kp* value of 36.10 L/g-Fe for HFO at our experimental conditions. This value is 28% higher than the *Kp* we obtained for ICS but is in the same order of magnitude. The corresponding surface excess of 0.064 mg/m^2 is, however, lower than calculated by the DDL model as Dzombak and Morel (1991) consider a theoretical SSA of 600 m^2/g for HFO, which is higher than the BET surface area of ICS. Nevertheless, we consider the possibility that based on the DDL model the *Kp* value could be adjusted to other conditions by determining the relative effect of P distribution when changing pH or ionic strength. Next to pH and ionic strength, the equilibrium distribution coefficient can be affected by the presence of ions such as organic matter, sulfate, carbonates, silicates, and arsenate competing with phosphate for surface sites (Grafe et al., 2002; Hiemstra, 2018; Liu et al., 2018; Mendez and Hiemstra, 2019) and should be taken into consideration when treating natural waters. Also temperature is expected to effect both equilibrium concentrations and rate constants, but the temperature effect is out of the scope of this study.

4.3. Implications for practical applications

The contribution of slow sites to P adsorption has practical consequences for the design, operation, and lifespan of ICS filters. Integrating stop-flow periods in the operation of filters allows the regeneration of fast adsorption sites, but the resting times have to be sufficient for P to be transferred to slow sites. We tested five different operation scenarios: (i) continuous flow, (ii) resting 3 months a year (during summer time), (iii) resting 1 week and (iv) 2 weeks per month, for a 40x40x40 cm filter with 4 L/h flow and 1 mg/L inflow water. The target is to keep concentrations below 0.15 mg/L. The scenarios are not strictly comparable, scenarios (ii) and (iii) treat the same volume, 75% of the total volume in scenario (i). Scenarios (ii) and (iii) demonstrate the contributions of slow kinetics and the effect of different lengths in the resting periods on P retention. To make the treated volume in scenario (iv) comparable to scenario (i), we assumed that 2 filter compartments (of the given dimensions) are used with alternating resting periods every 2 weeks. Fig. 5 displays the P concentrations in the effluent for all scenarios.

Scenario (ii) exhibits a larger recovery than scenario (iii), this effect is reached because the resting period is longer. Nevertheless, after 24.000 h (2 years in operation) they both reach a comparable final concentration of about 0.15 mg/L and retain a similar mass of P for the same treated volume, about 0.065 kg P. Comparing scenarios (i) and (iv) with the same treated volume, the continuous filter scenario (i) needs to be replaced three times in five years (every 1.65 years) to meet the 0.15 mg/L target. Instead, scenario (ii) can meet the target using only two filters and alternating operation every 2 weeks. Making use of two filters scenario (ii) retains 0.342 kg while scenario (i) retains 0.167 kg P using three filters in five years.

5. Summary and conclusion

A quantitative model for phosphate adsorption on ICS was developed, which was able to account for slow adsorption reactions, with the

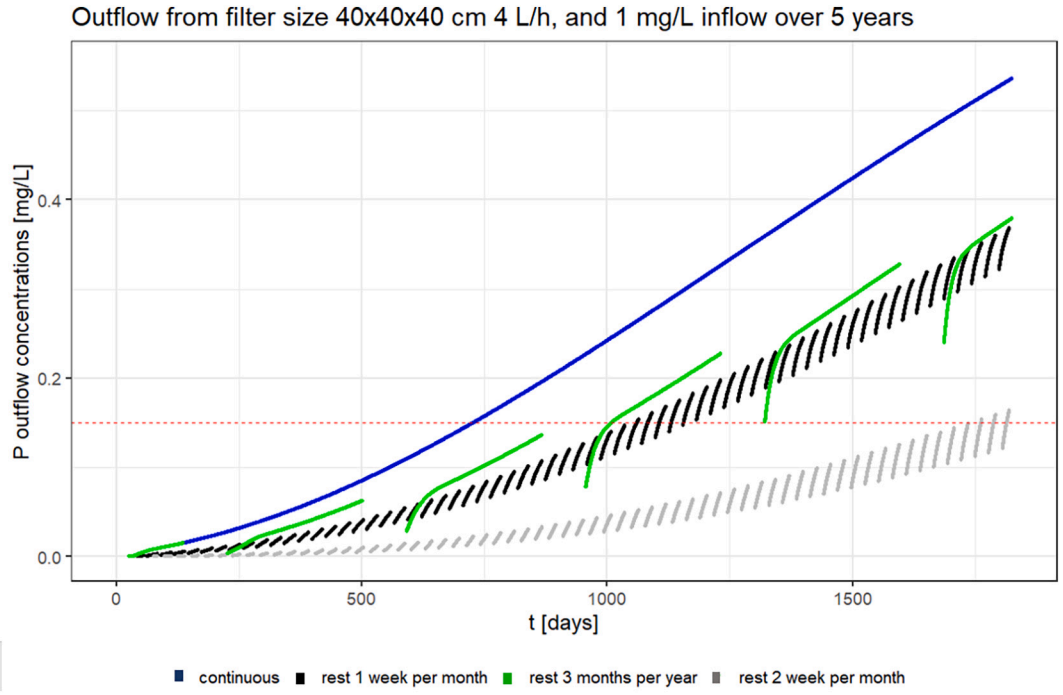

Fig. 5. P outflow concentrations for practical example of a 5-year ICS filter operation with 4 different operative scenarios:: (i) continuous flow, (ii) resting 3 months a year (during summer time), (iii) resting 1 week and (iv) 2 weeks per month. The dashed red line indicates the target outflow concentration, 0.15 mg/L.

intention to provide a tool for optimizing the application of ICS filters. The conceptual two-site model including transport-limited adsorption kinetics was supported by electron microscopic analyses of ICS. Long-term column experiments under several flow conditions were used to calibrate and validate the model. The model reproduced phosphate concentration of continuous and intermittent flow conditions, as well as adsorption and desorption. Adsorption proceeded rapidly on a small number of sites (4.5%) and is described with a linear equilibrium adsorption model. Adsorption on most sites proceeded slowly on the time scale of months, which we related to intra-particle diffusion. The calculated maximum adsorption capacity under experimental conditions was 47.7 mg/g-Fe, or 0.084 mg/m^2 at 1.70 mg-P/L inflow implying an equilibrium partition coefficient of 28.1 L/g-Fe. The model was used to test how ICS filter operation can be optimized to exploit the high capacity of the slow adsorption. An example shows how introducing resting periods improve the phosphate removal and operation duration of ICS filters.

From your results we conclude:

- Phosphate adsorption on ICS takes place at two times scales: fast adsorbing sites at the outside of the grains and slow kinetic adsorption into the iron coating.
- Only 4.5% of sites are in equilibrium and represent fast-accessible sites.
- Optimal ICS filter operation contains recovery phases. Flow interruptions in the time scale of the slow adsorption process (weeks to months) can extend the filter operation time significantly.

Declaration of Competing Interest

The authors declare that they have no known competing financial interests or personal relationships that could have appeared to influence the work reported in this paper.

Data availability

The model and data are available on github: https://github.com/victoriabarcala/ICS_adsorptionmodel

Acknowledgments

This study was funded by P-TRAP (EU Grant No. 813438, Marie Skłodowska- Curie Actions). We like to thank Arcadis and Aquaminerals for the ICS. We like to acknowledge T.M. van Genuchten for his support with Stanmod, Karel As and Michael Thelen, and University Bayreuth for the BET analysis, Eric Hellebrand for SEM-EDX, and Erik van Vilsteren and Mingkai Ma for their support in building the column set-up.

Appendix A. Supplemental material

The supplementary material includes an image of the column set-up, a description of the analytical techniques, tracer test results of columns I, II, and III, sensitivity analysis of the parameters in Stanmod, more detailed BET-SSA results, and EDX spectra. The data set and model are available at https://github.com/victoriabarcala/ICS_adsorptionmodel. Supplementary data to this article can be found online at https://doi.org/10.1016/j.jconhyd.2023.104160.

References

Ajmal, Z., Muhmood, A., Usman, M., Kizito, S., Lu, J., Dong, R., Wu, S., 2018. Phosphate removal from aqueous solution using iron oxides: adsorption, desorption and regeneration characteristics. J. Colloid Interface Sci. https://doi.org/10.1016/j.jcis.2018.05.084.

Barcala, V., Rozemeijer, J., Osté, L., Van Der Grift, B., Gerner, L., Behrends, T., 2020. Processes controlling the flux of legacy phosphorus to surface waters at the farm scale. Environ. Res. Lett. 16 (1) https://doi.org/10.1088/1748-9326/abcdd4.

Barcala, V., Stefan, J., Jan, G., Stefan, M., Andreas, V., Thilo, B., 2022. Phosphorus adsorption on iron-coated sand under reducing conditions. J. Environ. Qual. https://doi.org/10.1002/jeq2.20432.

Bieroza, M., Bergström, L., Ulén, B., Djodjic, F., Tonderski, K., Heeb, A., Svensson, J., Malgeryd, J., 2019. Hydrologic extremes and legacy sources can override efforts to mitigate nutrient and sediment losses at the catchment scale. J. Environ. Qual. 48 (5), 1314–1324. https://doi.org/10.2134/jeq2019.02.0063.

Bol, R., Gruau, G., Mellander, P.E., Dupas, R., Bechmann, M., Skarbøvik, E., Bieroza, M., Djodjic, F., Glendell, M., Jordan, P., Van der Grift, B., Rode, M., Smolders, E., Verbeeck, M., Gu, S., Klumpp, E., Pohle, I., Fresne, M., Gascuel-Odoux, C., 2018. Challenges of reducing phosphorus based water eutrophication in the agricultural landscapes of Northwest Europe. Front. Mar. Sci. 5 (AUG), 1–16. https://doi.org/10.3389/fmars.2018.00276.

Boujelben, N., Bouzid, J., Elouear, Z., Feki, M., Jamoussi, F., Montiel, A., 2008. Phosphorus removal from aqueous solution using iron coated natural and engineered sorbents. J. Hazard. Mater. 151 (1), 103–110. https://doi.org/10.1016/j.jhazmat.2007.05.057.

Bromly, M., Hinz, C., Aylmore, L.A.G., 2007. Relation of dispersivity to properties of homogeneous saturated repacked soil columns. Eur. J. Soil Sci. February, 293–301. https://doi.org/10.1111/j.1365-2389.2006.00839.x.

Chardon, Groenenberg, J.E., Temminghoff, E.J.M., Koopmans, G.F., 2012. Use of reactive materials to bind phosphorus. J. Environ. Qual. 41 (3), 636–646. https://doi.org/10.2134/jeq2011.0055.

Chardon, W., Groenenberg, J.E., Vink, J.P.M., Voegelin, A., Koopmans, G.F., 2021. Use of iron-coated sand for removing soluble phosphorus from drainage water. Sci. Total Environ. 815, 152738 https://doi.org/10.1016/j.scitotenv.2021.152738.

Das Gupta, M., Loganathan, P., Vigneswaran, S., 2012. Adsorptive removal of nitrate and phosphate from water by a Purolite ion exchange resin and hydrous ferric oxide columns in series. Separat. Sci. Technol. (Philadelphia) 47 (12), 1785–1792. https://doi.org/10.1080/01496395.2012.658487.

De Klein, J.J.M., Koelmans, A.A., 2011. Quantifying seasonal export and retention of nutrients in west European lowland rivers at catchment scale. Hydrol. Process. 25 (13), 2102–2111. https://doi.org/10.1002/hyp.7964.

Dupas, R., Tittel, J., Jordan, P., Musolff, A., Rode, M., 2018. Non-domestic phosphorus release in rivers during low-flow: mechanisms and implications for sources identification. J. Hydrol. 560, 141–149. https://doi.org/10.1016/j.jhydrol.2018.03.023.

Dzombak, D.A., Morel, F.M.M., 1991. Surface Complexation Modeling: Hydrous Ferric Oxide. Wiley.

Fiorellino, N., Kratochvil, R., Coale, F., 2017. Long-term agronomic drawdown of soil phosphorus in mid-Atlantic coastal plain soils. Agron. Soils Environ. Quality. https://doi.org/10.2134/agronj2016.07.0409.

Fraters, B., Hooijboer, A., Vrijhoef, A., Plette, A., van Duijnhoven, N., Rozemeijer, J., Gosseling, M., Daatselaar, C., Roskam, J., Begeman, H. (2021). Agricultural practices and water quality in the Netherlands : status (2016-2019) and trends (1992-2019).

Grafe, M., Eick, M.J., Grossl, P.R., Saunders, A.M., 2002. Adsorption of arsenate and arsenite on ferrihydrite in the presence and absence of dissolved organic carbon. J. Environ. Qual. 1123 (31), 1115–1123. https://doi.org/10.2134/jeq2002.1115.

Groenenberg, J.E., Chardon, W.J., Koopmans, G.F., 2013. Reducing phosphorus loading of surface water using iron-coated sand. J. Environ. Qual. 42 (1), 250–259. https://doi.org/10.2134/jeq2012.0344.

Gu, S., Gruau, G., Dupas, R., Rumpel, C., Crème, A., Fovet, O., Gascuel-Odoux, C., Jeanneau, L., Humbert, G., Petitjean, P., 2017. Release of dissolved phosphorus from riparian wetlands: evidence for complex interactions among hydroclimate variability, topography and soil properties. Sci. Total Environ. 598 (May), 421–431. https://doi.org/10.1016/j.scitotenv.2017.04.028.

Hiemstra, T., 2018. Ferrihydrite interaction with silicate and competing oxyanions: geometry and hydrogen bonding of surface species. Geochim. Cosmochim. Acta 238, 453–476. https://doi.org/10.1016/j.gca.2018.07.017.

Hong, S.U., Ouyang, L., Bruening, M.L., 2009. Recovery of phosphate using multilayer polyelectrolyte nanofiltration membranes. J. Membr. Sci. 327 (1–2), 2–5. https://doi.org/10.1016/j.memsci.2008.11.035.

Ippolito, J.A., Barbarick, K.A., Elliott, H.A., 2011. Drinking water treatment residuals: a review of recent uses. J. Environ. Qual. 40 (1), 1. https://doi.org/10.2134/jeq2010.0242.

Jentzsch, T.L., Penn, R.L., 2006. Influence of aluminum doping on ferrihydrite nanoparticle reactivity. J. Phys. Chem. 110, 11746–11750. https://doi.org/10.1021/jp060957.

Jerez, J., Flury, M., 2006. Humic acid-, ferrihydrite-, and aluminosilicate-coated sands for column transport experiments. Colloids Surf. A Physicochem. Eng. Asp. 273 (1–3), 90–96. https://doi.org/10.1016/j.colsurfa.2005.08.008.

Koopmans, Gerwin F., Chardon, W.J., de Willigen, P., Van Riemsdijk, W.H., 2004. Phosphorus desorption dynamics in soil and the link to a dynamic concept of bioavailability. J. Environ. Qual. 33 (33), 1393–1402.

Koopmans, G.F., Hiemstra, T., Vaseur, C., Chardon, W.J., Voegelin, A., Groenenberg, J.E., 2020. Use of iron oxide nanoparticles for immobilizing phosphorus in-situ: increase in soil reactive surface area and effect on soluble phosphorus. Sci. Total Environ. 711, 135220 https://doi.org/10.1016/j.scitotenv.2019.135220.

Kronvang, B., Vagstad, N., Behrendt, H., Bøgestrand, J., Larsen, S.E., 2007. Phosphorus losses at the catchment scale within Europe: an overview. Soil Use Manag. 23 (Suppl. 1), 104–116. https://doi.org/10.1111/j.1475-2743.2007.00113.x.

Lambert, N., Van Aken, P., Van den Broeck, R., Dewil, R., 2020. Adsorption of phosphate on iron-coated sand granules as a robust end-of-pipe purification strategy in the horticulture sector. Chemosphere 267, 129276. https://doi.org/10.1016/j.chemosphere.2020.129276.

Lewis, J., Sjöstrom, J., 2010. Optimizing the experimental design of soil columns in saturated and unsaturated transport experiments ☆. J. Contam. Hydrol. 115 (1–4), 1–13. https://doi.org/10.1016/j.jconhyd.2010.04.001.
Liu, A.R., Chi, L., Wang, X., Sui, Y., 2018. Review of metal (Hydr)oxide and other adsorptive materials for phosphate removal from water ruiting. J. Environ. Chem. Eng. https://doi.org/10.1016/j.jece.2018.08.008.
Lucas, E.R., Toor, G.S., Mcgrath, J.M., 2021. Agronomic and environmental phosphorus decline in coastal plain soils after cessation of manure application. Agric. Ecosyst. Environ. 311 (January), 107337 https://doi.org/10.1016/j.agee.2021.107337.
Maroto, J.A., de Dios, J., de las Nieves, F.J., 2002. Use of a Mariotte bottle for the experimental study of the transition from laminar to turbulent flow. Am. J. Phys. 70 (7), 698–701. https://doi.org/10.1119/1.1469038.
Mendez, J.C., Hiemstra, T., 2019. Carbonate adsorption to ferrihydrite: competitive interaction with phosphate for use in soil systems. ASC Earth Space Chem. 3, 129–141. https://doi.org/10.1021/acsearthspacechem.8b00160.
Moelants, N., Smets, I.Y., Van Impe, J.F., 2011. The potential of an iron rich substrate for phosphorus removal in decentralized wastewater treatment systems. Sep. Purif. Technol. 77 (1), 40–45. https://doi.org/10.1016/j.seppur.2010.11.017.
Morel, F.M., Hering, J.G., 1993. Principles and Applications of Aquatic Chemistry. John Wiley & Sons.
Murphy, J., Riley, J.P., 1962. A modified single solution method for the determination of phosphate in natural waters. Anal. Chim. Acta 27 (C), 31–36. https://doi.org/10.1016/S0003-2670(00)88444-5.
Mystrioti, C., Papassiopi, N., Xenidis, A., Dermatas, D., Chrysochoou, M., 2015. Column study for the evaluation of the transport properties of polyphenol-coated nanoiron. J. Hazard. Mater. 281, 64–69. https://doi.org/10.1016/j.jhazmat.2014.05.050.
Nur, T., Johir, M.A.H., Loganathan, P., Nguyen, T., Vigneswaran, S., Kandasamy, J., 2014. Phosphate removal from water using an iron oxide impregnated strong base anion exchange resin. J. Ind. Eng. Chem. 20 (4), 1301–1307. https://doi.org/10.1016/j.jiec.2013.07.009.
Penn, C., Bryant, R.B., Callahan, M.P., Mcgrath, J.M., 2011. Use of industrial by-products to sorb and retain phosphorus. Commun. Soil Sci. Plant Anal. 42 (6), 633–644. https://doi.org/10.1080/00103624.2011.550374.
Penn, C., Chagas, I., Klimeski, A., Lyngsie, G., 2017. A review of phosphorus removal structures: how to assess and compare their performance. Water (Switzerland) 9 (8), 1–22. https://doi.org/10.3390/w9080583.
Penn, C., Livingston, S., Shedekar, V., King, K., Williams, M., 2020. Performance of field-scale phosphorus removal structures utilizing steel slag for treatment of subsurface drainage. Water (Switzerland) 12 (2). https://doi.org/10.3390/w12020443.
Pérez-López, R., Nieto, J.M., de Almodóvar, G.R., 2007. Utilization of fly ash to improve the quality of the acid mine drainage generated by oxidation of a sulphide-rich mining waste: Column experiments. Chemosphere 67 (8), 1637–1646. https://doi.org/10.1016/j.chemosphere.2006.10.009.
Rittmann, B.E., Mayer, B., Westerhoff, P., Edwards, M., 2011. Capturing the lost phosphorus. Chemosphere 84 (6), 846–853. https://doi.org/10.1016/j.chemosphere.2011.02.001.
Rozemeijer, J.C., Klein, J., Broers, H.P., Van Tol-Leenders, T.P., Van der Grift, B., 2014. Water quality status and trends in agriculture-dominated headwaters; a national monitoring network for assessing the effectiveness of national and European manure legislation in the Netherlands. Environ. Monit. Assess. 186 (12), 8981–8995. https://doi.org/10.1007/s10661-014-4059-0.
Schoumans, O.F., Chardon, W.J., Bechmann, M.E., Gascuel-Odoux, C., Hofman, G., Kronvang, B., Rubæk, G.H., Ulén, B., Dorioz, J.M., 2014. Mitigation options to reduce phosphorus losses from the agricultural sector and improve surface water quality: a review. Sci. Total Environ. 468–469, 1255–1266. https://doi.org/10.1016/j.scitotenv.2013.08.061.
Sharma, S., Petrusevski, B., Schippers, J.C., 2002. Characterisation of coated sand from iron removal plant. Water Sci. Technol. 2 (2), 247–257. https://doi.org/10.2166/ws.2002.0070.
Sharpley, A., Jarvie, H.P., Buda, A., May, L., Spears, B., Kleinman, P., 2013. Phosphorus legacy: overcoming the effects of past management practices to mitigate future water quality impairment. J. Environ. Qual. 42 (5), 1308–1326. https://doi.org/10.2134/jeq2013.03.0098.
Simunek, J., van Genuchten, M.T., Sejna, M., Toride, N., Leij, F.J., 1999. The STANMOD Computer Software for Evaluating Solute Transport in Porous Media Using Analytical Solutions of Convection-Dispersion Equation. ARS, USDA.
Soetaert, K., Herman, P., 2009. A Practical Guide to Ecological Modelling Using R as a Simulation Platform.
Soetaert, K., Meysman, F., 2012. Environmental modelling & software reactive transport in aquatic ecosystems: rapid model prototyping in the open source software R. Environ. Model. Softw. 32, 49–60. https://doi.org/10.1016/j.envsoft.2011.08.011.
Soetaert, K., Petzoldt, T., 2010. Solving differential equations in R: package de solve. J. Stat. Softw. 33 (9) https://doi.org/10.18637/jss.v033.i09.
Stoll, S., Frossard, E., Stamm, C., Prasuhn, V., 2021. The time it takes to reduce soil legacy phosphorus to a tolerable level for surface waters: what we learn from a case study in the catchment of Lake. Geoderma 403. https://doi.org/10.1016/j.geoderma.2021.115257.
Stoner, D., Penn, C., McGrath, J., Warren, J., 2012. Phosphorus removal with by-products in a flow-through setting. J. Environ. Qual. 41 (3), 654–663. https://doi.org/10.2134/jeq2011.0049.
Suresh Kumar, P., Prot, T., Korving, L., Keesman, K.J., Dugulan, I., van Loosdrecht, M.C. M., Witkamp, G.J., 2017. Effect of pore size distribution on iron oxide coated granular activated carbons for phosphate adsorption – Importance of mesopores. Chem. Eng. J. 326, 231–239. https://doi.org/10.1016/j.cej.2017.05.147.
Toride, N., Leij, F.J., Van Genuchten, M.T., 1995. The CXTFIT code for estimating transport parameters from laboratory or field tracer experiments. Res. Rep, Res. R (137), 1–138. http://www.researchgate.net/publication/247824027_The_CXTFIT_Ver_2.0._Code_for_estimating_transport_parameters_from_laboratory_or_field_tracer_experiments.
Van Beek, C.G.E.M., Dusseldorp, J., Joris, K., Huysman, K., Leijssen, H., Schoonenberg Kegel, F., De Vet, W.W.J.M., Van De Wetering, S., Hofs, B., 2016. Contributions of homogeneous, heterogeneous and biological iron(II) oxidation in aeration and rapid sand filtration (RSF) in field sites. J. Water Supply: Res. Technol. - AQUA 65 (3), 195–207. https://doi.org/10.2166/aqua.2015.059.
Van Beek, C.G.E.M., Hofman-Caris, C.H.M., Zweere, G.J., 2020. Drinking water treatment and chemical well clogging by iron(II) oxidation and hydrous ferric oxide (HFO) precipitation. J. Water Supply: Res. Technol. - AQUA 69 (5), 427–437. https://doi.org/10.2166/aqua.2020.140.
Van Genuchten, M., Simunek, J., Leij, F.J., Toride, N., 2012. Stanmod: model use, calibration and validation. Am. Soc. Agricult. Biol. Eng. 55 (4), 1353–1366.
Vandermoere, S., Ralaizafisoloarivony, N.A., Van Ranst, E., De Neve, S., 2018. Reducing phosphorus (P) losses from drained agricultural fields with iron coated sand (–glauconite) filters. Water Res. 141, 329–339. https://doi.org/10.1016/j.watres.2018.05.022.
Wang, Li, W., Harrington, R., Liu, F., Parise, J.B., Feng, X., Sparks, D.L., 2013. Effect of ferrihydrite crystallite size on phosphate adsorption reactivity. Environ. Sci. Technol. 47 (18), 10322–10331. https://doi.org/10.1021/es401301z.
Willett, I.R., Chertres, C.J., Nguyen, T.T., 1988. Migration of phosphate into aggregated particles of ferrihydrite. J. Soil Sci. 39 (2), 275–282. https://doi.org/10.1111/j.1365-2389.1988.tb01214.x.
Withers, P.J.A., Neal, C., Jarvie, H.P., Doody, D.G., 2014. Agriculture and eutrophication: where do we go from here? Sustainability (Switzerland) 6 (9), 5853–5875. https://doi.org/10.3390/su6095853.
Zhang, Y., 2008. Geochemical Kinetics. Princeton University Press.
Zhang, R., Wang, L., Hussain Lakho, F., Yang, X., Depuydt, V., Igodt, W., Quan Le, H., Rousseau, D.P.L., Van Hulle, S., 2022. Iron oxide coated sand (IOS): scale-up analysis and full-scale application for phosphorus removal from goat farm wastewater. Sep. Purif. Technol. 284 (November 2021), 120213 https://doi.org/10.1016/j.seppur.2021.120213.